



OPEN ACCESS INTERNATIONAL JOURNAL OF SCIENCE & ENGINEERING

COMBUSTION SYNTHESIS OF ZnO NANO PARTICLES USING EUPHORBIA TIRUCALLI LATEX AS REDUCING AGENT AND STUDY OF ITS STRUCTURAL AND PHOTOLUMINESCENCE CHARACTERISATION

M.S.Geetha^{1*}, H. N. Shivananjaiah²

Vijaya Composite College, Bangalore, 560 011, India.¹

Government Science College, Nrupatunga road, Bangalore, 560 001, India.²

geethashivu33@gmail.com

Abstract: Multifunctional ZnO nanoparticles were synthesised by combustion methods using *Euphorbia tirucalli* plant latex as reducing agent. SEM and TEM images shows that the particles are spherical in shape. XPS and FTIR confirms purity of the sample. Energy gap of the semiconducting ZnO nano particles was found to be 2.98 eV through UV-vis spectroscopic studies. Photo luminescence studies shows that the particles exhibit prominent green emission due to intrinsic defects. CIE plot indicates the usability of the particles in white light emitting diode (LED). The report concludes a simple, eco friendly, fast, cost effective method for the synthesis of ZnO nanoparticles.

Keywords: Multi functional ZnO; *Euphorbia tirucalli*; SEM with EDX; XPS; PL studies.

I INTRODUCTION

ZnO is a key technological material. Zinc oxide is a unique material that exhibits dual properties like semiconducting and piezoelectric property. The strong piezoelectric and pyroelectric properties are due to lack of a centre of symmetry in wurtzite, combined with large electromechanical coupling. Nano structured ZnO materials have received broad attention due to their distinguished performance in electronics, optics and photonics. ZnO is visible light transparent and can be made highly conductive by suitable doping. ZnO is a versatile functional material that has a diverse group of growth morphologies, such as nano combs, nano rings, nano helices/nano springs, nano belts, nano wires and nano cages [1-3]. The objective of this article is to review the unique ZnO nanostructures and the study of its structural mechanisms and optical properties. There are several synthesis methods for the preparation of ultrafine nano oxide like hydrothermal, sol gel, emulsion precipitation, salvo thermal, combustion *etc* [4-9]. But from last few years green mediated synthesis has received much attention, as it is eco friendly, cost effective. Our team is mainly working on green mediated synthesis of most useful nano oxides using different parts of plants like flowers, fruits, seeds, leaves, bark and

latex. Actually, latex in the plant is its biological waste, sometimes it uses it for its protection against pests. In some cases, if the latex is taken in small amounts, it can have medicinal applications also. Use of plant parts avoids the accumulation of unwanted chemicals on its surface thus by extending its applications to the field of medicine. It is well known that purity of ZnO is important for its application [9-11], demanding extreme thermal treatment after its synthesis. So the synthesised compound was calcinated at 750 °C. In our earlier work [12] we have reported that the size and morphology of the nanoparticles depends mainly of fuel concentration, which is also supported by our present work.

II EXPERIMENTAL AND CHARACTERIZATION

In the present report, we followed the same synthesis method as in our earlier report [12], but took the latex of *Euphorbiacea tirucalli*. Hydrated Zinc Nitrate, Zn(NO₃)₂ was procured from Sigma-Aldrich and used as starting materials without further purification. Latex of *E. tirucalli* was used as fuel for synthesis of ZnO nano particles. In a typical synthesis 2, 4 and 6ml of crude latex were dissolved in 8-10 ml of double distilled water. To each 1g of Zinc Nitrate was added and mixed well using magnetic stirrer for approximately 5-10 min and then placed in a preheated

muffle furnace maintained at $450 \pm 10^\circ$ C. The reaction mixture boils froths and thermally dehydrates forming foam. The entire process was completed in less than 30 min. Further, the final white powder was kept for calcination at a temperature of 750° C for two hr in the muffle furnace.

Surface morphology and elemental composition was characterized using SEM (Hitachi-S4700) with inbuilt EDS and transmission electron microscope (TEM, TECNAI F-30) respectively. PXRD patterns were obtained using advanced powder X-ray Diffractometer (using $\text{Cu K}\alpha = 1.54056 \text{ \AA}$ radiation). FTIR spectra for all the samples were recorded using Bomem Hartmann & Braun, MB-series. UV-vis spectra were recorded using Lambda-35 PerkinElmer spectrophotometer in the wavelength range 200-800 nm. PL studies were carried out using Flurolog-3 spectro fluorimeter (JobinYvon USA) at RT. The phosphor was excited at 394 nm and emission spectra were recorded in the range 450-800 nm with the help of grated PMT detector.

III RESULTS AND DISCUSSION

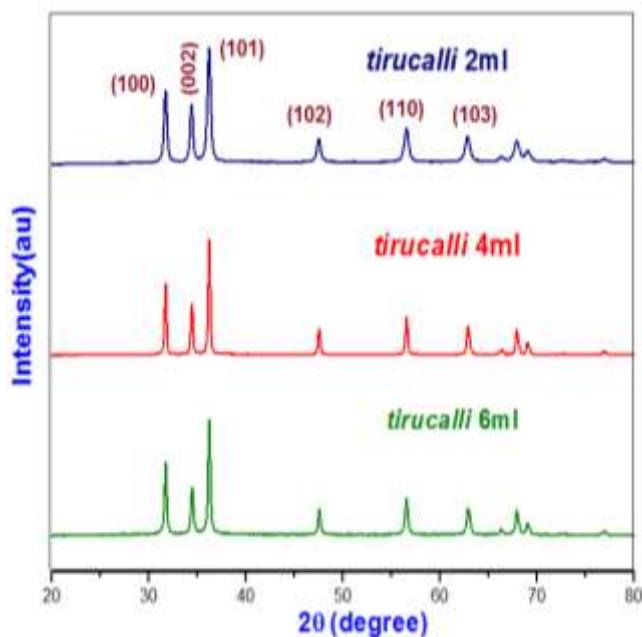


Figure 1 PXRD patterns of ZnO using different plant latex concentration

Fig 1 shows PXRD pattern of ZnO prepared by combustion method using *E.tirucalli* as reducing agent. Sharp peaks in the PXRD pattern indicates that the particles were well crystallised. Maximum intensity peaks were observed at (hkl) values (100), (002), (101), (102), (110), (103). Maximum intensity peak was observed at (101) (hkl) values. This implies that most of the particles in the plane are have (101) plane. The (hkl) values were obtained by Rietveld refinement. The average crystallite size was determined by taking full width half deflection method and using Scherrer equation $D = 0.9\lambda / \beta_{hkl} \cos\theta$ where β_{hkl} represents FWHM intensity, λ is the wave length of X rays and 2θ is the

diffracting angle. The average crystallite size, strain, dislocation density and stress were tabulated in Table 1.

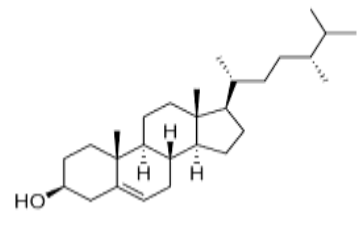
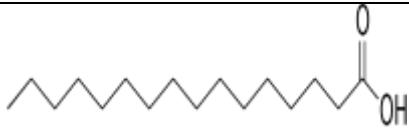

Table 1: Crystallite size, strain, Dislocation density and stress of ZnO nano particles prepared by various concentration of E-tirucalli plant milky latex.

Sample ZnO (ml)	Scherrer Equation D(nm)	Strain $\epsilon \times 10^{-3}$	Dislocation density $\delta = 1/D^2 \times 10^{15}$	Stress $\sigma = \epsilon Y \times 10^6 \text{ Nm}^{-2}$
6	15.3101	2.243	4.1488	313
4	25.0252	1.412	1.9509	206
2	29.2533	1.197	1.4388	179

From the table it is clear that, as the latex volume decreases, the particle size increases and strain decreases. *Euphorbia* family mainly includes flowering plants. *Euphorbia tirucalli* is one of the most important tree Euphorbias, known worldwide for its medicinal uses like used as a remedy for ailments such as: spleen enlargement, asthma, dropsy, leprosy, biliousness, leucorrhoea, dyspepsia, jaundice, colic, tumors, and bladder stones and many other uses include curving of wooden crafts, production of fuel wood, timber production, use as hedge plants, use in re-forestation programs and others. *E. tirucalli* contains white milky latex in any part of the shoot. Main composition of *E.tirucalli* latex and its composition [14] is shown in Table 2. During combustion process, gases which are evolved carry the heat by hindering the size of the ZnO particles. As the latex volume in the sample increases, more gases evolved carry the heat resulting in smaller size of the particles. Smaller size of the particles results in more strain.

Table 2: Chemical composition and their structural formula of E.tirucalli plant milky latex.

NAME	STRUCTURE
Sitosterol	
Stigmasterol	

Campesterol	
Palmitic acid	
Linoleic acid	

The structural details of ZnO were obtained by Rietveld refinement using Fullprof software (Fig 2) and packing diagram was done using VESTA software. The Rietveld method refines user-selected parameters to minimize the difference between an experimental pattern (observed data) and a model based on the hypothesized crystal structure and instrumental parameters (calculated pattern) using Full profile fitting and crystallographic constraints. Rietveld refinement is more popular as it uses directly the measured intensities points of the entire spectrum (as wide as possible), less sensible to model errors and less sensible to experimental errors. Ideal powder diffraction patterns can be simulated by knowing the space group symmetry, unit cell dimensions, atom types, relative coordinates of atoms in unit cell, atomic site occupancies and atomic thermal displacement parameters. For simulation profile shape function Pseudo-Voigt function was chosen which is given by $V = \eta L + (1 - \eta)G$, ($0 \leq \eta \leq 1$) where Lorentzian $L = I_0 [1 + ((2\theta - 2\theta_0)/\omega)^2]^{-\eta}$ and Gaussian $G = I_0 \exp [-\ln 2 ((2\theta - 2\theta_0)/\omega)^2]$. Quality of refinement was specified by R - structure factor, $R_F = \frac{\sum (I_k^{obs} - I_k^{calc})}{\sum I_k^{obs}}$, R - Bragg factor, $R_B = \frac{\sum (I_k^{obs} - I_k^{calc})}{\sum I_k^{obs}}$, R - weighted pattern $R_{wp} = [\sum W(Y^{obs} - Y^{calc})^2 / \sum W(Y^{obs})^2]^{1/2}$ and Goodness of fit $\chi^2 = R_{wp}/R_{exp}$. Table 3 gives the structural details of ZnO obtained by Rietveld refinement. It was found that, for all the samples, crystal system was hexagonal with Laue class 6/m and point group 6. As the particle size decreases a, b, c values found to decrease with the corresponding decrease in the cell volume [48.14 (Å)³ to 47.99 (Å)³]. Atomic coordinates of Zn and O were recorded in Table 3. The GOF was nearly 1.3 indicating very good agreement between the experimental and calculated pattern. Using the data obtained by Rietveld

refinement and VESTA software packing diagram was drawn and shown in Fig 3.

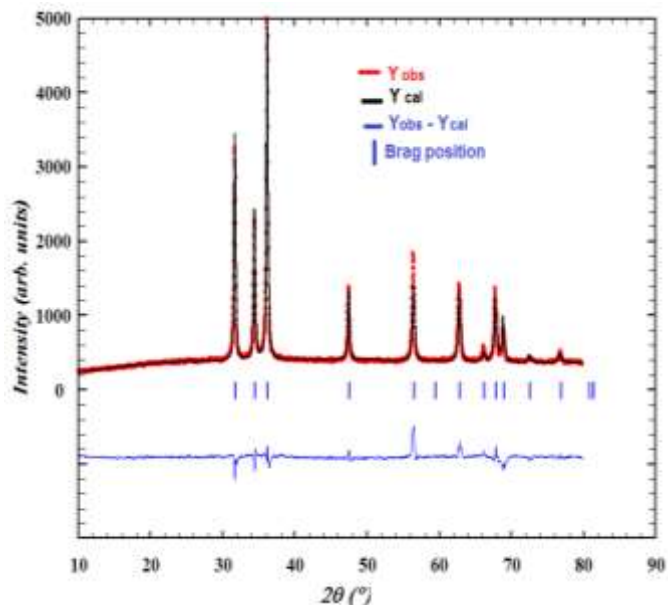


Figure 2 : Rietveld refinement of ZnO (6ml latex)

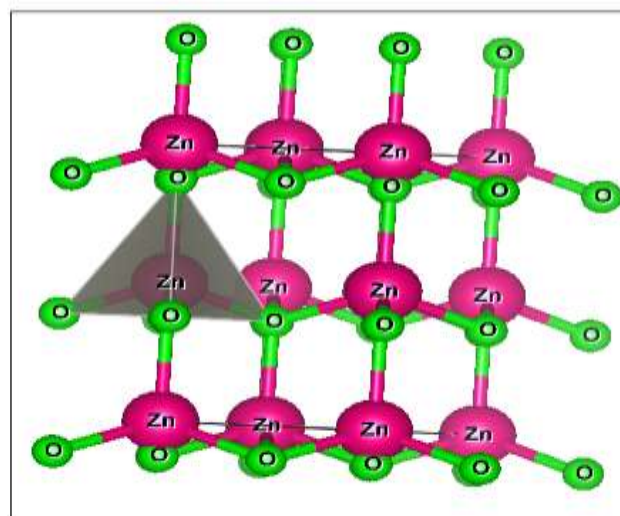


Fig 3 : Packing diagram of ZnO

The morphological features were studied using SEM and TEM. Fig 4 (a, b, c) shows the SEM pictures of ZnO (2– 6 ml tirucalli latex).The particles appear to be almost spherical in shape and highly agglomerated. The average particle size was estimated using ImageJ, which is well consistent with those values obtained by Scherrer’s equation. As fuel concentration increases, particle size found to decrease and the agglomeration will also reduce.

Table 3: Rietveld refinement of ZnO

	Tirucalli 2ml	Tirucalli 4ml	Tirucalli 6ml
Crystal system	Hexagonal	Hexagonal	Hexagonal
Laue class	6/m	6/m	6/m
Point group	6	6	6
Bravis Lattice	P	P	P
Lattice symbol	hP	hP	hP
Cell parameters			
a=b	3.265833	3.262582	3.260596
c	5.223163	5.220798	5.212503
$\alpha=\beta$	90	90	90
γ	120	120	120
a/c	0.6252	0.62492	0.625532
Direct cell volume(A³)³	48.1490	48.1272	47.9922
Atomic coordinates			
Zn	0.3333	0.3333	0.3333
x	0.6666	0.6666	0.6666
y	0.03563	0.03563	0.00795
z	2.31809	2.62244	2.71017
B	0.76598	0.76598	0.76677
Occupancy			
O	0.3333	0.3333	0.3333
x	0.6666	0.6666	0.6666
y	0.41965	0.41985	0.39191
z	26.80184	24.96463	26.80184
B	2.08678	2.07234	2.18383
Occupancy			
Rp	3.55	4.43	3.78
R wp	4.83	6.3	5.45
R exp	3.82	4.66	4.66
χ^2	1.6	1.82	1.37
GOF index	1.3	1.4	1.2
Density of compound (g/cc)	7.516	7.499	7.678



Figure 4 : SEM images of ZnO (a) 2ml (b) 4ml and (c) 6ml latex.

Fig 5 (a) and 5 (b) shows TEM and SAED images of ZnO prepared using 6ml tirucalli latex. TEM images clearly evident that the particles were nearly spherical and average particle size was around 50nm. Further, the polycrystalline in nature clearly evident in selected area electron diffraction pattern (SAED). The SAED pattern clearly indicates (100), (002), (101), (102) and (110) planes. The spherical nature of particles can be explained by vesicle-template mechanism [15] (Fig 6). During combustion initially latex froths and then catches fire. During this process gases comes out of the sample, carrying the additional heat, which hinders the growth of ZnO particles. The quantity of the gases depends on the composition of latex, which in turn results with different morphology to the sample. In our earlier report [12], we have reported hexagonal morphology to ZnO particles. In this report, we obtained spherical shaped particles.

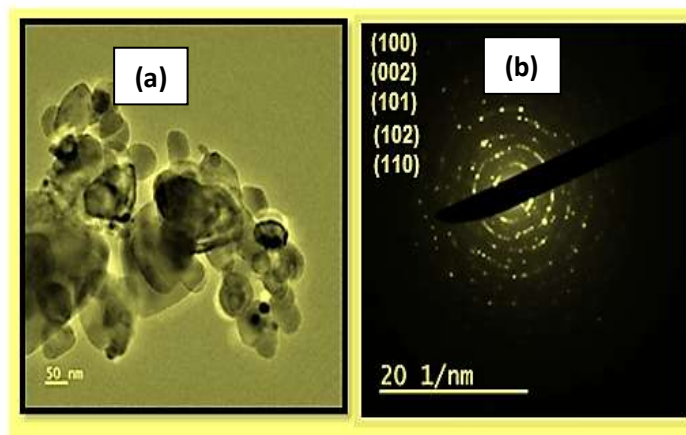


Figure 5 : TEM images and SAED of ZnO prepared with 6ml latex.

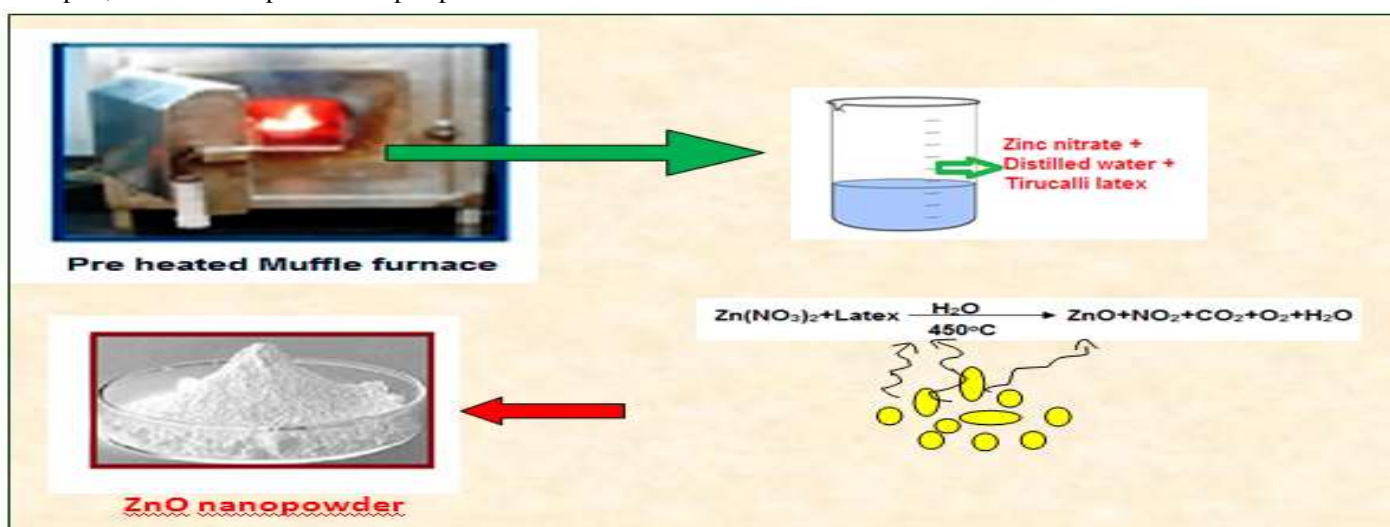


Figure 6 : Schematic representation of formation process spherical morphology of ZnO

Fig 7 shows the XPS spectrum of a ZnO. The NPs consist of Zn and O. A trace amount of carbon (7d) in the results was mainly attributed to the adventitious hydrocarbon from XPS itself [16]. Fig 7b and 7c shows the high resolution XPS spectra of the elements of Zn and O. The deconvolution of the O 1S region of the XPS spectrum indicates that it can be fit by the two peaks at 531.44eV and 533.5 eV. The less intense low energy component at 531.44 eV was attributed to O₂⁻ ions in ZnO and an intense high energy component at 533.5 eV was attributed to hydroxyl species present on the surface of the NPs [17]. In Fig 7b, the peaks located at 997.44 eV and 9770.38 eV were associated to Zn 2P_{3/2} and Zn 2P_{1/2} respectively.

The formation of nano crystalline ZnO prepared using tirucalli latex as fuel was investigated using FTIR spectra (Fig 8). The absorption peaks appearing around 3485 cm⁻¹ of ZnO was attributed to -OH stretching vibrations of adsorbed water molecule [18]. The frequency band at 1636 cm⁻¹ may be related to amide I bonds associated with

proteins or vibrations due to C-C functional groups from heterocyclic compounds [19]. The peak at 1410 cm⁻¹ could be appearing due to stretching vibrations of C- N functional groups of amines and C- O bonds of water soluble heterocyclic compounds such as alkaloids and flavones [20]. The characteristic peak of ZnO was around 508 cm⁻¹. The FTIR measurement proves the presence of carboxylic and free amino groups adhered on the surface of various morphologies of ZnO despite calcination at 750 °C. The amino and carboxylic groups observed in FTIR could be considered to bind with surface NPs and thus provide stability to the growth of ZnO by preventing the agglomeration. The functional bonds such as C-C, C-N and C-O derived from water soluble alkaloids and flavones from the tirucalli latex may also be observed to provide capping action and assist in the stabilization process of NPs growth. Finally, the amino, carboxylic and phenol functional groups of tirucalli latex could be responsible for the formation of various morphologies of ZnO.

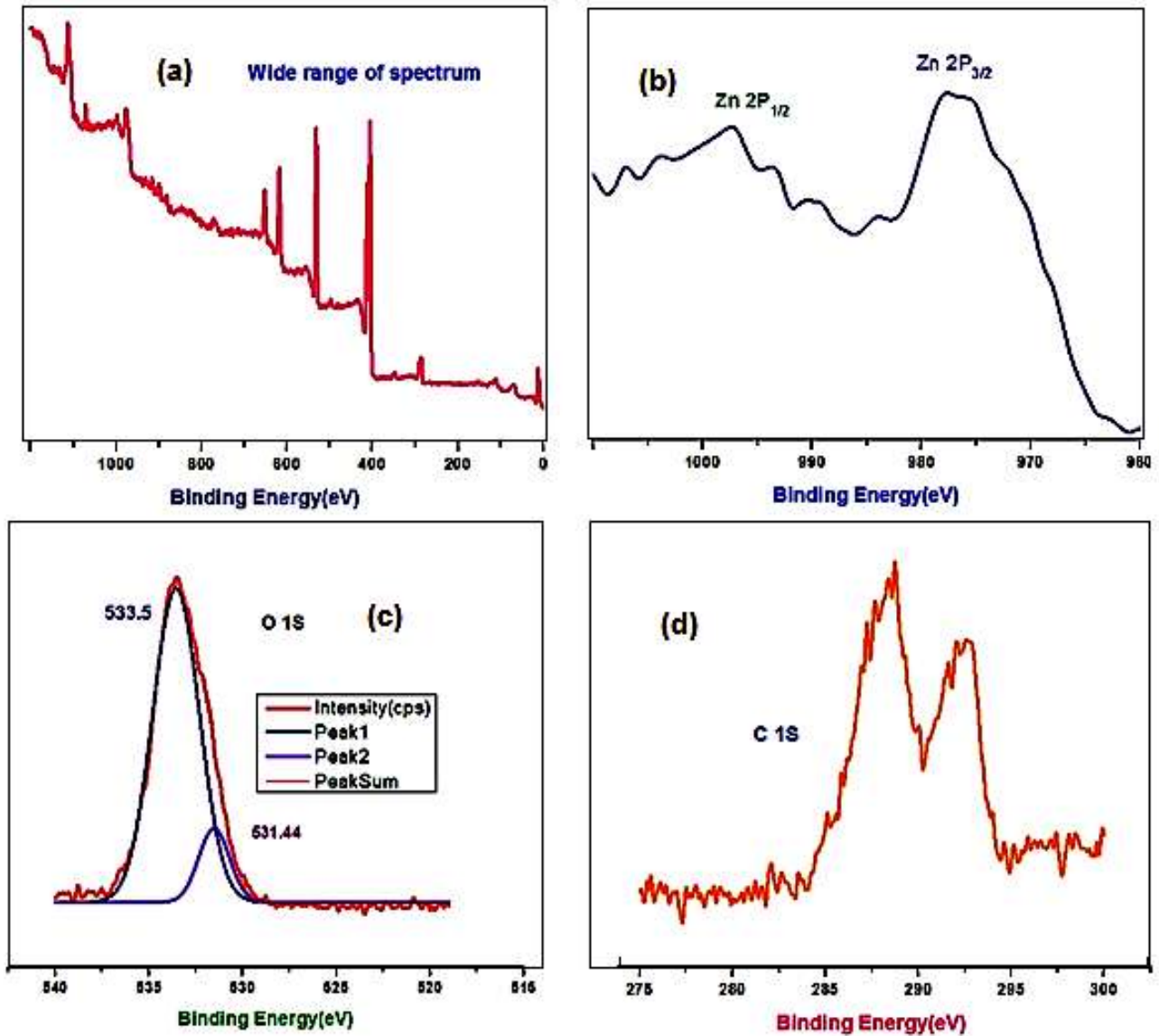


Figure 7: XPS spectra of Zn , O and C

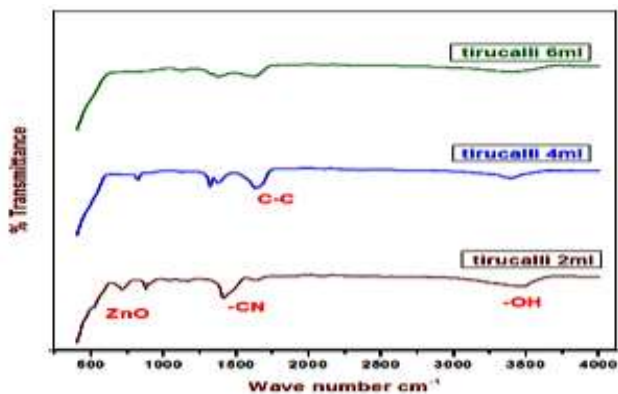


Figure 8 : FTIR of ZnO

The optical characterization of the ZnO was recorded on UV-Vis absorption spectrophotometer. Fig 9 shows the UV-Visible absorption spectra of ZnO nanoparticles as a function of absorbance versus wavelength. The UV-Visible absorption spectroscopy of ZnO nanoparticles prepared using Tirucalli latex as fuel shows an exciton absorption peak at about 416 nm. The corresponding energy gap $E_g = hc/\lambda$ which is about 2.98 eV. As the particle size decreases, we observed red shift in the adsorption peak, which indicates slight increase in the band gap energy[21]. As the particle size decreases, increase in the energy gap may be due to quantum confinement effect[22].

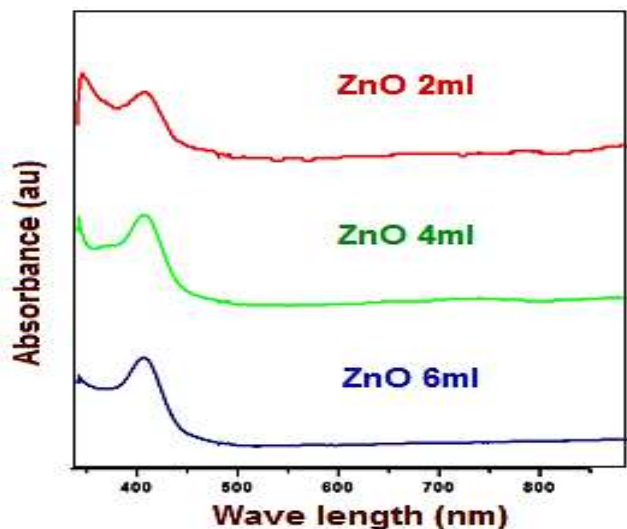


Figure 9 : UV Visible spectra of ZnO

PL study gives us the fundamental information about energy levels lying within the band gap states. The PL emission infers the efficacy of charge carrier trapping, migration and also the fate of photo generated electron-hole pairs in the materials. The recombination of excited electron-hole pair was the result of PL emission and hence efficient charge carrier separation resulted in lower PL intensity. PL spectra of ZnO (2ml, 4ml and 6 ml) excited at a photon energy of 550nm (2.25 eV) are presented in Fig 10. The emission spectra shows clear emission peaks at 434 nm, 486 nm, 539 nm and 652 nm . It is well established that bulk and ZnO nano particles exhibit three PL peaks, a UV near band-edge emission peak around 400 nm, a green emission near 520 nm and a red emission in the vicinity of 650 nm [23-25]. In our earlier work [12] on similar band around 400nm peak has been ascribed to exciton–exciton scattering process from the $n = 1$ state to the exciton continuum state (P-line). The transitions are shown in Fig 11. While the broad emission observed near 539 nm is assigned to oxygen vacancies (V_O) [26]. The broad green-yellow band near 486 nm is due to deep level emissions in green region, which is ascribed to oxygen vacancies, zinc interstitials or zinc vacancies [27]. The presence of defects was due to appreciable bond breaking and surface stress caused by large

Surface to volume ratio. In the present study we have observed UV near band edge emission peak around 400 nm and visible emission in the 486–540 nm peaks are frequently originating luminescent peaks reported in all ZnO samples. Thus, the results of the present study are in excellent agreement with earlier reports on nano particles[21-27]. It should be noted that the appearance of sharp, narrow UV emission splitting into two is an indication of better crystallinity and good quality of ZnO nano powder growth [28] which is in excellent agreement with the PXRD and SEM results.

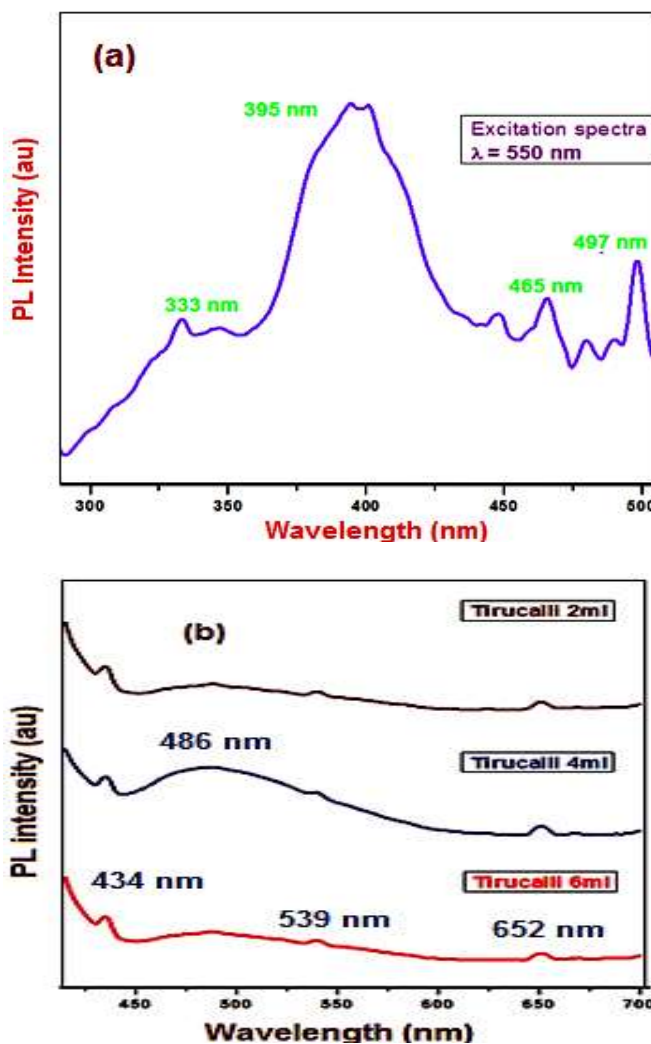


Figure 10 : Excitation and emission spectra of ZnO.

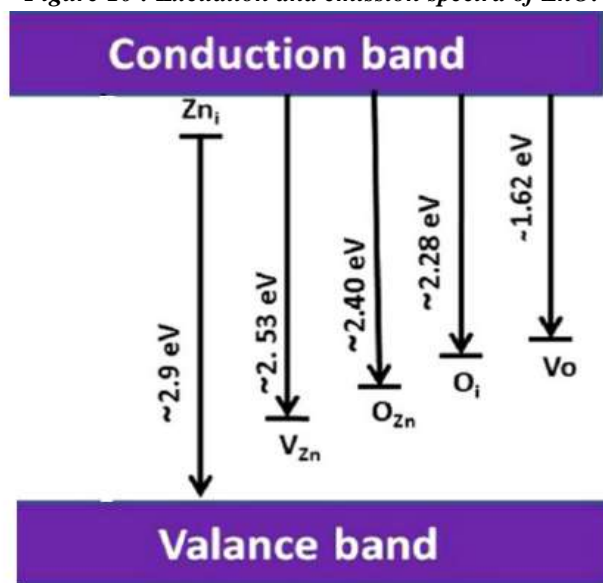


Figure 11 : Typical energy level diagram of ZnO.

The Commission International De I-Eclairage (CIE) chromaticity coordinates for ZnO (2ml, 4ml, 6ml) was shown

in Fig 12. Coordinated color temperature can be estimated by Planckian locus, which is only a small portion of the (x, y) chromaticity diagram and there exist many operating points outside the Planckian locus. If the coordinates of a light source do not fall on the Planckian locus, the coordinated color temperature (CCT) was used to define the color temperature of a light source. CCT was calculated by transforming the (x, y) coordinates of the light source to (U₀, V₀) by using following equations, and by determining the temperature of the closest point of the Planckian locus to the light source on the (U₀, V₀) uniform chromaticity diagram.

$$U' = \frac{4x}{-2x+12y+3} \text{ and } V' = \frac{9y}{-2x+12y+3}$$

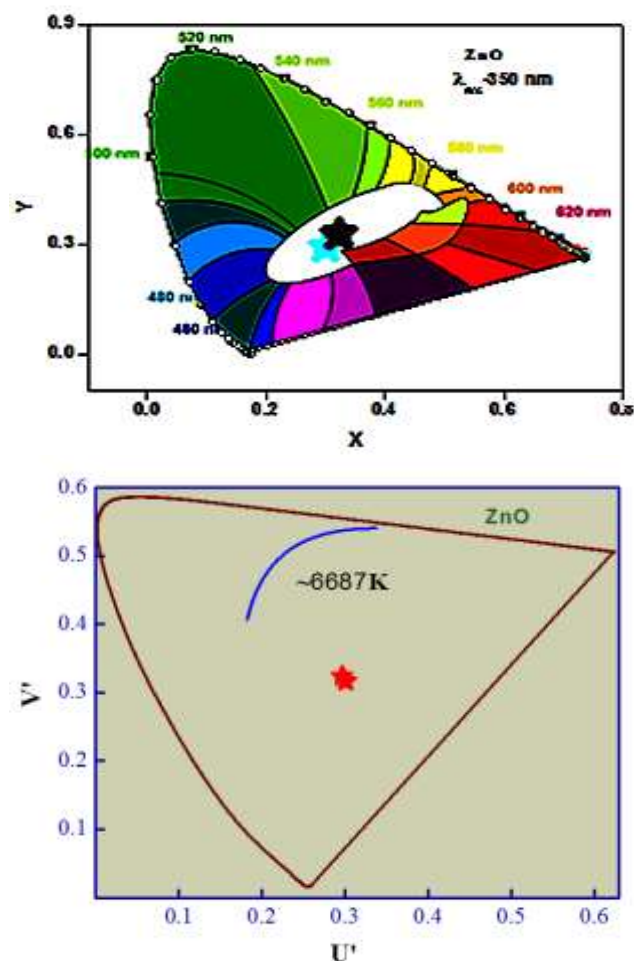


Figure 12 : CCT and CIE plot of ZnO.

IV Conclusion

A series of white light emitting ZnO (2ml, 4ml and 6ml latex) nanophosphors were prepared by green mediated combustion method. The hierarchical superstructures largely depend on latex concentration of tirucalli. The growth mechanism of spherical, hierarchical superstructures was proposed. The PXRD patterns of phosphors calcined at 750 °C confirms single phase of ZnO. The energy gap (E_g) was around 2.98 eV. The phosphor exhibit intense white

emission. PL intensity is maximum at 4 ml latex and then diminishes due to self-quenching effect. Further, the phosphor showed CIE chromaticity co-ordinates and CCT values which are very close to the values of standard white phosphors. Hence, the phosphor obtained by green mediated combustion method may be useful for display and solid state lighting applications.

References

[1] C. Sun, B.P. Uberuaga, L. Yin, J. Li , Y. Chen , M.A. Kirk , M. Li , S.A. Maloy, H. Wang, C. Yu , X. Zhang , Resilient ZnO nanowires in an irradiation environment: An in situ study, *Acta Materialia* 95 (2015) 156–163.

[2] Moghaddam, A.B., Nazari, T., Badraghi, J. and Kazemzad M. (2009) Synthesis of ZnO nanoparticles and electrodeposition of polypyrrole/ZnO nanocomposite film. *Int J Electrochem Sci*, 4, 247–257.

[3] Shokuhfar, T., Vaezi, M.R., Sadrnezhad, S.K. and Shokuhfar, A. (2008) Synthesis of zinc oxide nanopowder and nanolayer via chemical processing. *Int J Nanomanufacturing*, 2, 149-162.

[4] Kim, S.-J. and Park, D.-W. (2007) Synthesis of ZnO nanopowder by thermal plasma and characterization of photocatalytic property. *Appl Chem*, 11, 377-380.

[5] Vaezi, M.R. and Sadrnezhad, S. (2007) Nanopowder synthesis of zinc oxide via solochemical processing. *Mater Design*, 28, 515–519.

[6] Ge, M.Y., Wu, H.P., Niu, L., Liu, J.F., Chen, S.Y., Shen, P.Y., Zeng, Y.W., Wang, Y.W., Zhang, G.Q. and Jiang, J.Z. (2007) Nanostructured ZnO: from monodisperse nanoparticles to nanorods. *J Cryst Growth*, 305, 162–166.

[7] Hambrock, J., Rabe, S., Merz, K., Birkner, A., Wohlfart, A., Fischer, R.A. and Driess, M. (2003) Low-temperature approach to high surface ZnO nanopowders and a non-aqueous synthesis of ZnO colloids using the single- source precursor [MeZnOSiMe₃]₄ and related zinc siloxides. *J Mater Chem*, 13, 1731–1736.

[8] Kwon, Y.J., Kim, K.H., Lim, C.S. and Shim, K.B. (2002) Characterization of ZnO nanopowders synthesized by the polymerized complex method via an organochemical route. *J Ceram Process Res*, 3, 146-149.

[9] Z. Y. Fan and J. G. Lu, *J. Nanosci. Nanotechnol.*, 2005, 5, 1561.

[10] U. Ozgur, Y. I. Alivov, C. Liu, A. Teke, M. A. Reshchikov, S. Dogan, V. Avrutin, S. J. Cho and H. Morkoc, *J. Appl. Phys.*, 2005, 98, 041301.

[11] G. C. Yi, C. R. Wang and W. I. Park, *Semicond. Sci. Technol.*, 2005, 20, S22

[12] M.S. Geetha , H. Nagabhushana , H.N. Shivananjaiiah , Green mediated synthesis and characterization of ZnO nanoparticles using Euphorbia Jatropa latex as reducing agent, *Journal of Science: Advanced Materials and Devices* , (2016) 301-310.

[13] Louis-Felix Nothias-Scaglia, Jean-Francois Gallard, Vincent Dumontet, Fanny Roussi, Jean Costa, Bogdan I. Iorga, Julien Paolini, Marc Litaudon, *Journal of Natural products*, 78(2015)2423–2431.

- [14] Julius Mwine, Patrick Van Damme, Bernadetta Rina Hastilestari, Jutta Papenbrock, American Chemical Society, 27(2013)1127.
- [15] M. Venkataravanappa, H. Nagabhushana, G.P. Darshan, B. Daruka Prasad, G.R. Vijayakumar, H. B. Premkumar, Udayabhanu, Novel EGCG assisted ultrasound synthesis of self-assembled Ca_2SiO_4 : Eu^{3+} hierarchical superstructures: Photometric characteristics and LED applications, *Ultrasonics Sonochemistry*, (2016)315-321.
- [16] M. Chandrasekhar, H. Nagabhushana, Y.S. Vidya, K.S. Anantharaju, S.C. Sharma, H.B. Premkumar, S.C. Prashantha, B. Daruka Prasad, C. Shivakumarai, Rohit Sarafi, Synthesis of Eu^{3+} -activated ZnO superstructures: Photoluminescence, Judd–Ofelt analysis and Sunlight photocatalytic properties, *Journal of Molecular Catalysis A: Chemical*, 409 (2015) 26–41.
- [17] J.G. Yu, X.X. Yu, *Environ. Sci. Technol.* 42 (2008) 4902–4907.
- [18] S.C. Pillai, J.M. Kelly, D.E. McCormack, P. O'Brien, R.J. Ramesh, *Mater. Chem.* 13 (2003) 2586–2590.
- [19] J. Huang, Q. Li, D. Sun, Y. Lu, Y. Su, X. Yang, H. Wang, Y. Wang, W. Shao, N. He, J. Hong, C. Chen, *Nanotechnology* 18 (2007) 105104.
- [20] R.A. Nyquist, R.O. Kagel, *Infrared Spectra of Inorganic Compounds*, Academic Press, New York, 1971, pp. 220.
- [21] H.B. Premkumar, B.S. Ravikumar, D.V. Sunitha, H. Nagabhushana, S.C. Sharma, M.B. Savitha, S. Mohandas Bhat, B.M. Nagabhushana, R.P.S. Chakradhar, Investigation of structural and luminescence properties of Ho^{3+} doped YAlO_3 nanophosphors synthesized through solution combustion route, *Spectrochimica Acta Part A: Molecular and Biomolecular Spectroscopy* 115 (2013) 234–243.
- [22] Krushiitha Shettya, S.V. Lokesh, Dinesh Rangappa, H.P. Nagaswarupa, H. Nagabhushana, K.S. Anantharaju, S.C. Prashantha, Y.S. Vidya, S.C. Sharma, Designing MgFe_2O_4 decorated on green mediated reduced graphene oxide sheets showing photocatalytic performance and luminescence property, *Physica B: Physics of Condensed Matter* (2016) 30545-2
- [23] Jianguo Zhou, Yali Wang, Fengying Zhao, Yingling Wang, Yan Zhang, Lin Yang, Photoluminescence of ZnO nanoparticles prepared by a novel gel-template combustion process, *Journal of Luminescence*, (2012)248-252.
- [24] P.B. Devaraja, D.N. Avadhani, S.C. Prashantha, H. Nagabhushana, S.C. Sharma, B.M. Nagabhushana, H.P. Nagaswarupa, H.B. Premkumar, $\text{MgO}:\text{Eu}^{3+}$ red nanophosphor: Low temperature synthesis and photoluminescence properties, *Spectrochimica Acta Part A: Molecular and Biomolecular Spectroscopy* 121 (2014) 46–52
- [25] Greta Patrinoiu, Jose Maria Calderon-Moreno, Carmen Mariana Chifiriuc, Crina Saviuc, Ruxandra Birjega, Oana Carp, Tunable ZnO spheres with high anti-biofilm and antibacterial activity via a simple green hydrothermal route, *Journal of Colloid and Interface Science* 462 (2016) 64–74.
- [26] M. Rakibuddin, Rajakumar Ananthakrishnan, Novel nano coordination polymer based synthesis of porous ZnO hexagonal nanodisk for higher gas absorption and photocatalytic activities, *Applied Surface Science* 362 (2016) 265–273.
- [27] D. Kavyashree, R. Ananda Kumari, H. Nagabhushana, S.C. Sharma, Y.S. Vidya, K.S. Anantharaju, B. Daruka Prasad, S.C. Prashantha, K. Lingaraju, H. Rajanaik, Orange red emitting Eu^{3+} doped Zinc oxide nanophosphor material prepared using *Guizotia abyssinica* seed extract: Structural and photoluminescence studies, *Journal of Luminescence* 167(2015)91–100.
- [28] M.A. Gondal, A.M. Ilyas, T.A. Fasasi, M.A. Dastageer, Z.S. Seddigi, T.F. Qahtan, M. Faiz, G.D. Khattak, Synthesis of green $\text{TiO}_2/\text{ZnO}/\text{CdS}$ hybrid nano-catalyst for efficient light harvesting using an elegant pulsed laser ablation in liquids method, *Applied Surface Science* 357 (2015) 2217–2222.